Tenth International Conference on Computational Fluid Dynamics (ICCFD10), Barcelona, Spain, July 9-13, 2018 **ICCFD10-334**

Role of Laminar Separation Bubbles on Airfoil at Low Reynolds Number in Martian Atmosphere

H. Zhan[*,**], J. Fang[***], A.Revell[**], S. Zhong[**], C. Moulinec[***], D. R. Emerson[***]and P. Bai[*]
zhlhazhu@hotmail.com

*China Academy of Aerospace Aerodynamics, 100074 Beijing, China
** School of Mechanical, Aerospace and Civil Engineering,
The University of Manchester, M13 9PL, UK
***Scientific Computing Department, STFC Daresbury Laboratory,
Warrington WA4 4AD, UK.

Abstract: Direct numerical simulation of flow over a triangular airfoil designed for the Martian atmosphere are performed at Reynolds numbers of $Re=3\times10^3$ and 1×10^4. The freestream Mach number is M=0.5, with the angles of attack changing from $\alpha=0°$ to 18° and $\alpha=0°$ to 11° respectively. The computations are performed using an in-house solver, ASTR, based on a compact sixth-order central scheme and tenth-order filter. The nonlinear variation of lift coefficients with angles of attack is observed at both Reynolds numbers. From the time-averaged flow fields obtained by three-dimensional simulations, it shows that the linear-to-nonlinear transition is caused by the transition of three separation forms around the triangular airfoil. At $Re=3\times10^3$, there is a recirculation zone that forms behind the apex for lower angles of attack, $\alpha\leq6°$. With an increase in the angle of attack ($\alpha=7°\sim8°$), a small separation bubble near the leading edge also appears, which we refer to as a double bubble separation. These two separation bubbles merge into a large leading-edge separation bubble when the angle of attack is increased to $\alpha=9°$. The effect of higher Reynolds numbers on flow fields around the airfoil is shifting the transition angle of attack to be lower. In the case of $Re=1\times10^4$, when $\alpha=5°$, two separation zones can be observed upstream and downstream of the apex, respectively.

Keywords: Direct Numerical Simulation, Low Reynolds Number, Laminar Separation Bubble, Airfoil.

1 Introduction

The unique atmospheric conditions of Mars require the wings and propellers of a Martian aircraft to operate at relatively low Reynolds numbers ($Re=10^3\sim10^5$) and moderately high Mach number (Ma=0.2~0.5). Therefore, an airfoil's performance has some specific characteristics, such as a nonlinear lift curve caused by the formation or burst of laminar separation bubbles (LSB) [1]. With the increasing interest in the design of aircraft for Mars, a precise prediction for the aerodynamic performance of an airfoil in Martian atmosphere and a clear understanding of the flow mechanism of LSB is required.

At present, numerical studies with high accuracy of the flow characteristics of airfoils are mostly focused on higher Reynolds numbers, such as 6×10^4 and under incompressible conditions. In the comprehensive study of Uranga *et al*. [1, 12], a high-order discontinuous Galerkin (DG) method for implicit large-eddy simulation (ILES) was introduced. More recently, ILES and Direct Numerical

Simulation (DNS) studies using the DG scheme have been conducted by Carton de Wiart & Hillewaert[3]. Numerical simulations by Galbraith & Visbal[4, 13, 14] have been conducted using a 6th-order accurate compact finite difference scheme with a high-order low-pass filter. Garmann & Visbal et al.[5] performed a comparative study of implicit and subgrid-scale models based large-eddy simulation with use of a 6th-order accurate compact finite difference scheme. Zhou & Wang[6] and Castonguay et al.[7] investigated the flow around the SD7003 using ILES with a spectral difference method for spatial discretization.

For flight on Mars, the assumption that the flow is incompressible, due to the relatively low Reynolds number, is not appropriate because of the low density atmospheric conditions. The objective of the present research is to perform DNS of flow over a triangular airfoil designed for the Martian atmosphere to investigate the aerodynamic characteristics of the airfoil at low Reynolds numbers, especially the laminar-turbulent transition through LSB around the critical angle of attack (AoA). The Reynolds numbers based on the freestream velocity, density, and the chord length simulated in this paper are $Re=3\times10^3$ and 1×10^4 with a freestream Mach number of $M=0.5$, and the AoA changing from $\alpha=0°$ to 18° and $\alpha=0°$ to 11°, respectively. The computations are performed using an in-house solver, ASTR, based on a compact sixth-order central scheme and tenth-order filter. From the flowfield obtained from DNS, the mechanism of how the flow structure of the laminar separation bubble influences the airfoil performance can be studied. Future Martian aircraft configuration design will benefit from such work.

2 Methodology

2.1 CFD Code

The current computations utilize the high-order DNS flow solver ASTR (Advanced flow Simulator for Turbulence Research). The characteristics of ASTR are as follows:

- High-order FDM on generalized mesh
  - High-order dealiasing compact central scheme
  - High-order low-dissipative shock-capturing scheme
  - 3rd-order Runge-Kutta time scheme
- Modern Fortran 90
- Parallelized by using MPI and hybrid MPI-OpenMP
- Collective HDF5 I/O
- Tested on ARCHER, Tianhe, Hector, Blue Gene…

The program structure of ASTR is shown in Figure 1. Figure 2 and Figure 3 are the scalability of ASTR and an example of well resolved wall-turbulence, respectively.

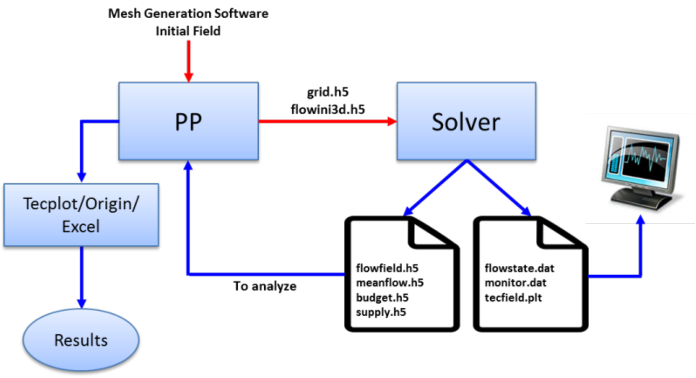

Figure 1: Program structure of ASTR.

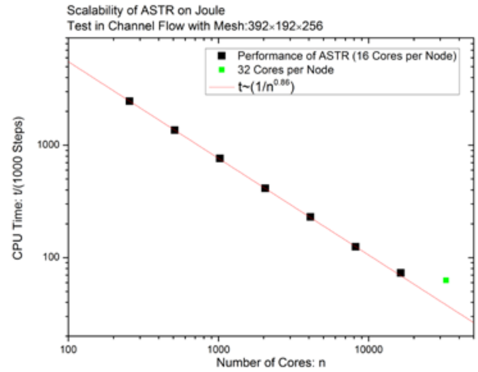

Figure 2: Scalability of ASTR.

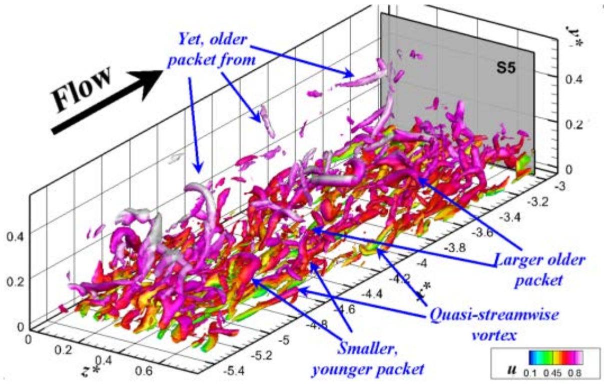

Figure 3: Well resolved wall-turbulence.

2.2 Airfoil

Based on an extensive aerodynamic characterization in incompressible flow [2], airfoils with sharp leading edges, flat surfaces, and even corrugation have been observed to exhibit high aerodynamic performance at low Reynolds numbers in the range of 10^3 to 10^4. The selected triangular airfoil here has a flat triangular cross section with its maximum thickness of 5% at the 30% chord c location, as shown in Figure 4. This particular airfoil is observed to possess high lift and high lift-to-drag ratio characteristics (L/D>9), and is one of the possible candidates for airfoils to be used in the design of propellers for Martian aircraft [3]. It should be noted that this airfoil is asymmetric.

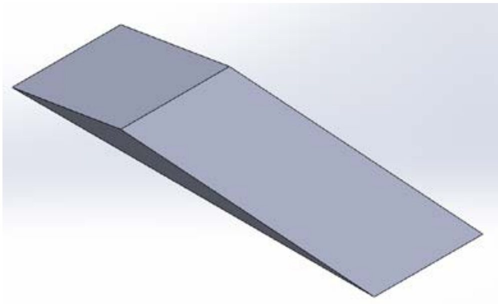

Figure 4: Triangular airfoil.

2.3 Computational Mesh

The baseline O-grid (Medium) was generated about the triangular airfoil with a rounded trailing edge, which had a radius of curvature of 0.0005 relative to the chord, shown in Figure 5. Grid coordinates are oriented such that ξ traverses clockwise around the airfoil, η is normal to the surface, and ζ follows the spanwise direction. The baseline mesh consisted of 371×201×97 points in the ξ, η, ζ directions, respectively, which contains 7.1 million hexahedral cells. The mesh is evenly spaced in the spanwise direction with a width of z/c=0.6. A spanwise periodic boundary condition was imposed on all meshes. The farfield boundary was positioned 30 chords away from the airfoil in order to reduce its influence on the solution near the airfoil.

Two additional meshes were generated to assess the effect of grid resolution. A coarse and a fine mesh were generated by altering the normal direction point count from 201 to 101 and 301 points, respectively. The coarse mesh consisted of 3.6 million while the fine mesh consisted of 10.7 million cells as shown in Table 1.

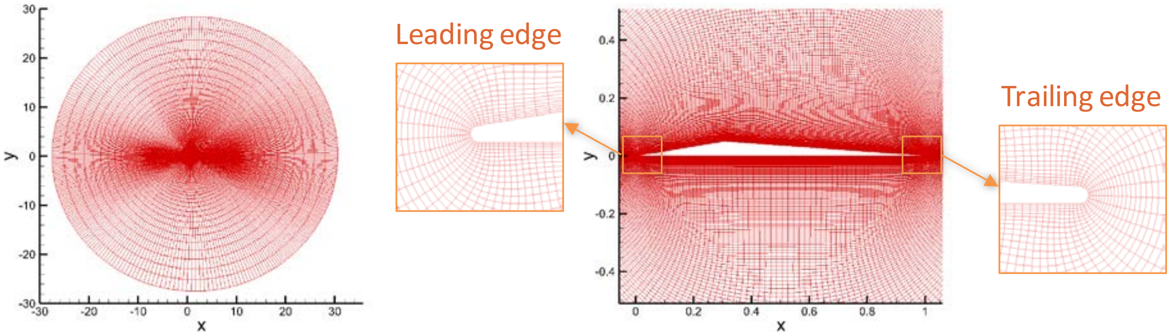

Figure 5: Baseline computational mesh with grid dimensions of 371×201×97.

Table 1: Computational mesh.

Grid	ξ	η	ζ	Cells
Coarse	371	101	97	3, 552, 000
Medium	371	201	97	7, 104, 000
Fine	371	301	97	10, 656, 000

2.4 Effect of Grid Resolution

Time-averaged flow fields and surface pressure coefficients for α=6° and α=12° at Re=3×10^3 obtained using ASTR with different meshes are compared in Figure 6 and Figure 7, respectively. Effects near the trailing edge motivated selection of the fine mesh.

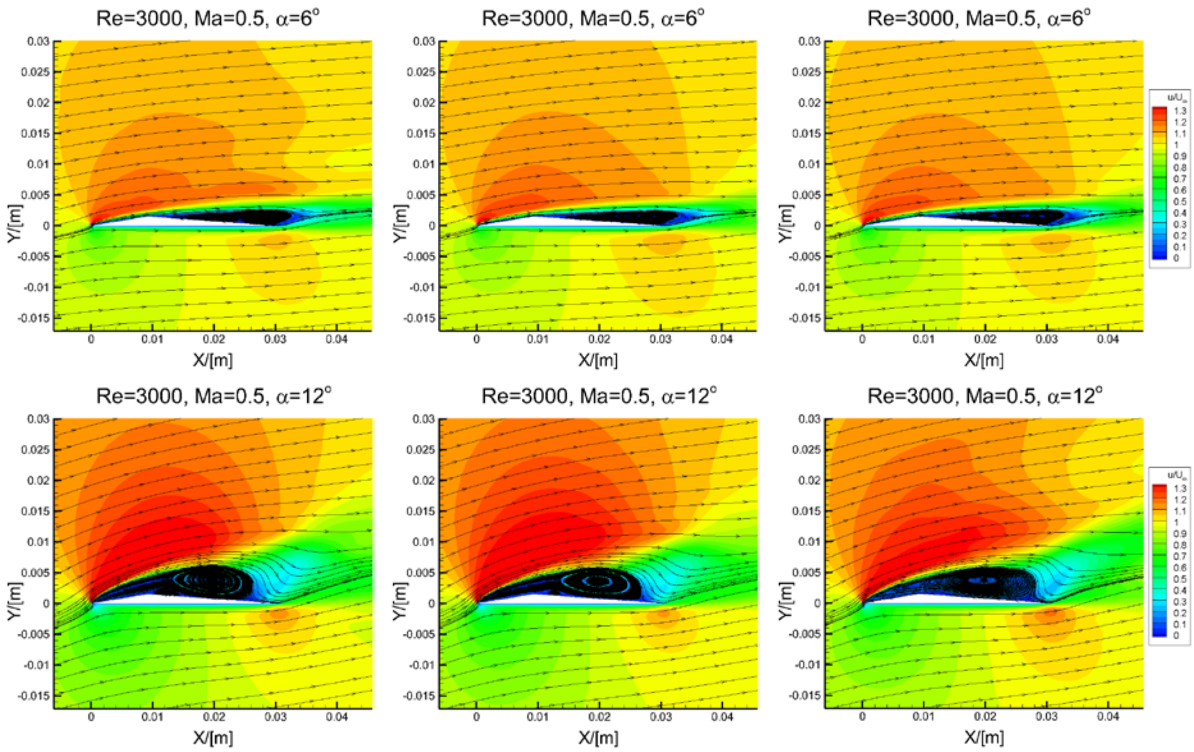

(a) Coarse (b) Medium (c) Fine

Figure 6: Effect of mesh resolution on time-averaged flow fields (Up: α=6°, down: α=12°).

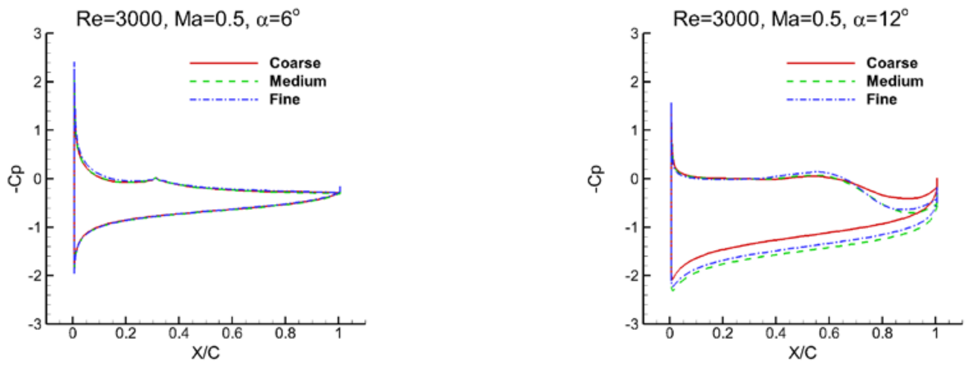

(a) α=6° (b) α=12°

Figure 7: Effect of mesh resolution on time-averaged pressure coefficients.

3 Results

3.1 Re=3×10^3

3.1.1 Two-dimensional simulations

Two-dimensional simulations were performed at Re=3×10^3 from angles of attack of α=0° to 18° (with increments in AoA given by Δα=3°). The lift and drag coefficients were computed by integrating the time-averaged pressure and skin friction over the surface of the airfoil. The integrated lift and drag coefficients are compared in Figure 8 with the computed values and experimental measurements of Munday et al [3]. It can be observed that for lower angles of attack of α≤9°, the present results match the DNS of Munday *et al*. well, but are higher than force measurements from the Mars wind tunnel (MWT). This may be caused by the difference in the spanwise direction between the computations (periodicity) and the experiments (walls).

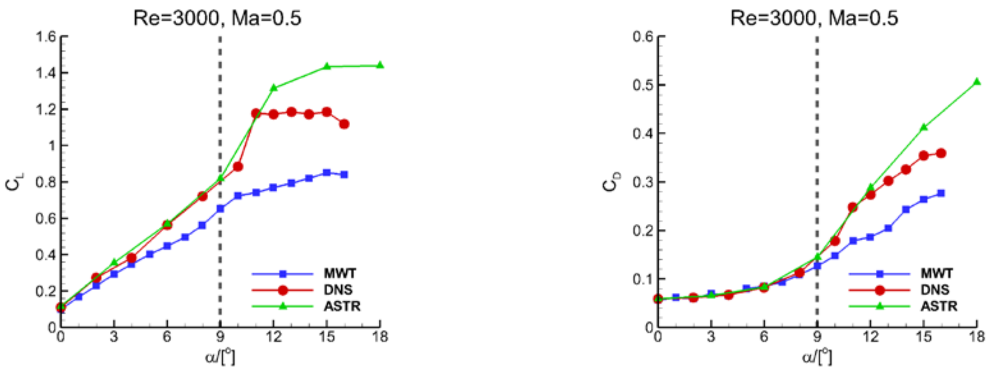

(a) C_L~α (b) C_D~α

Figure 8: Comparison of mean force coefficients with the results from reference [3] (Re=3×10^3).

Time-averaged flow fields presented in Figure 9 show that there is a recirculation zone that forms behind the apex for lower angles of attack of α≤6°. As the angle of attack increases to α=9°, a leading-edge vortex is observed that forms a recirculation region with reattachment upstream of the trailing edge. The recirculation zone grows and covers the majority of the airfoil for α=12°. The change of separation coincides with the linear-to-nonlinear lift transition as shown in Figure 8.

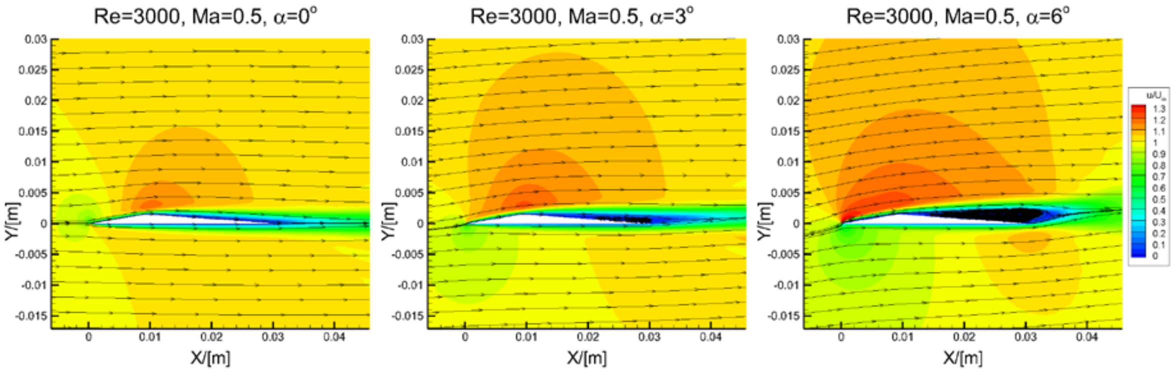

(a) Apex separation

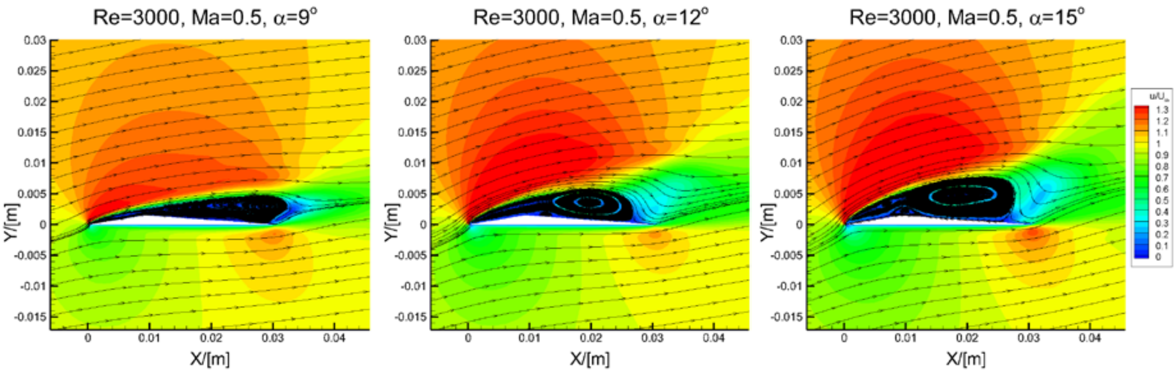

(b) Leading-edge separation

Figure 9: 2D time-averaged flow fields at Re=3×10^3 (α=0°~18°).

Time-averaged surface pressure coefficients for all the angles of attack computed are shown in Figure 10. Consistent with time-averaged flow fields, as the angle of attack increases, the suction surface pressure distribution shows two different forms with α=9° as a critical point.

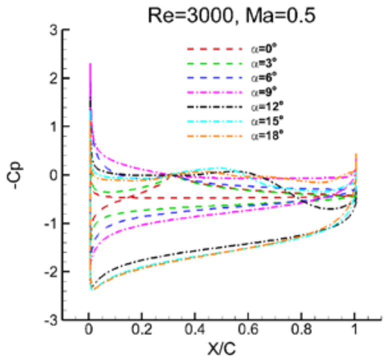

Figure 10: 2D time-averaged pressure coefficients at Re=3×10^3 (α=0°~18°).

3.1.2 Three-dimensional simulations

From the two-dimensional results, it can be observed that the critical point between apex separation and leading-edge separation is around α=9°, as shown in Figure 9. Based on this, three-dimensional DNS studies around α=9° with a spanwise domain size of 0.6c were carried out to find whether the critical point between the two separation zones is different from the two-dimensional results. Figure 11 shows the three-dimensional time-averaged flow fields at angles of attack of α=6° to 9° (Δα=1°). For α=6°, an apex separation bubble can be found on the airfoil, which is the same as the two-dimensional case. With the increase in angle of attack (α=7°~8°), it is interesting to note that a small separation bubble near the leading edge also appears but without the apex separation bubble. We refer to this separation phenomenon as a double bubble separation. These two separation bubbles merge into a large leading-edge separation bubble when angle of attack increases to α=9°.

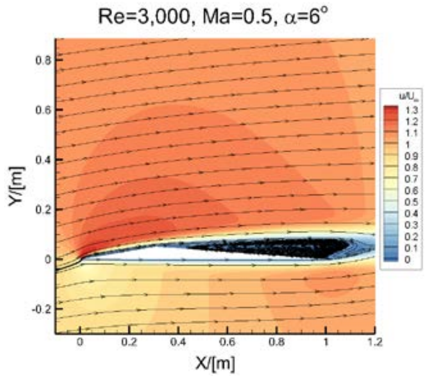

Apex separation

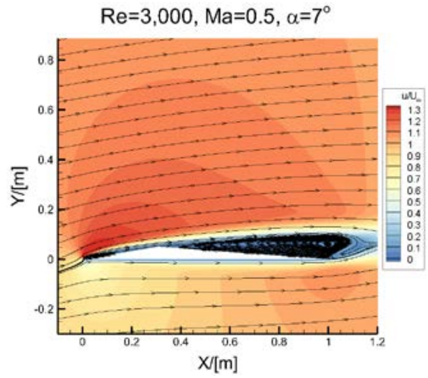

Double bubble separation

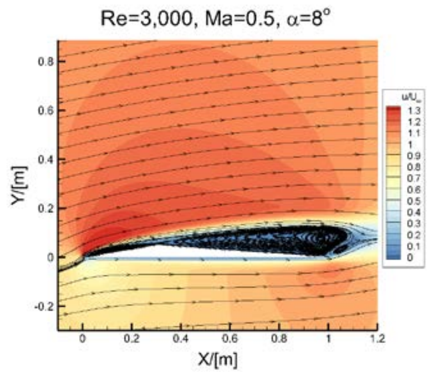

Double bubble separation

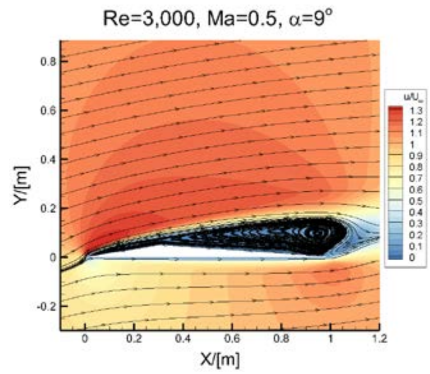

Leading-edge separation

Figure 11: 3D time-averaged flow fields at Re=3×10^3 (α=6°~9°).

3.2 Re=1×10^4

In order to analyze the effect of Reynolds number on the separation regions around the triangular airfoil, three-dimensional DNS at Re=1×10^4 from α=0° to 11° (Δα=1°) were conducted. Figure 12 shows the variations of the grid spacing in wall units in the circumferential, normal, and spanwise (*i*, *j*, *k*) directions along the upper and lower surface of the airfoil at α=9°. The maximum grid spacing in the *i*- and *z*-directions are below 18 and 9, respectively. The grid spacing in the *j*- direction (that is Δy^+) along the majority of the upper surface is below 1. Figure 13 shows the spatial grid in each direction around the airfoil. It shows that these grid distributions are sufficient to resolve the flow fields.

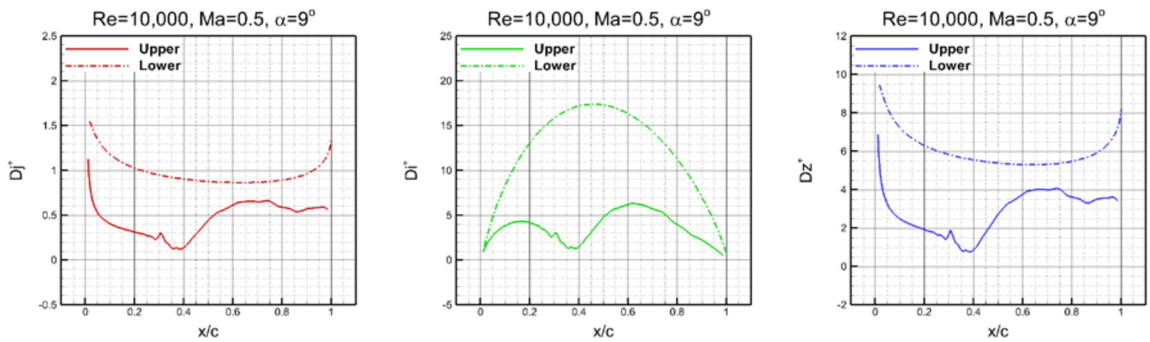

Figure 12: Wall mesh resolution (Re=1×10^4, α=9°).

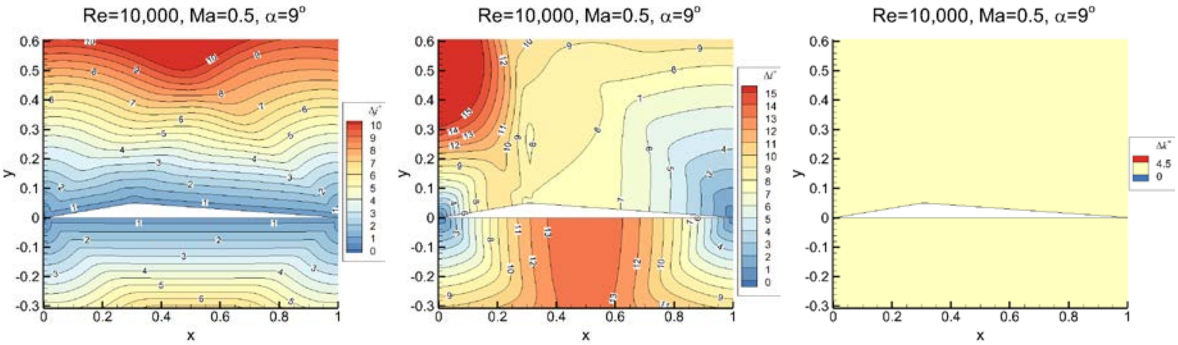

Figure 13: Spatial mesh resolution (Re=1×10^4, α=9°).

The variation of mean lift and drag coefficients with angles of attack is presented in Figure 14. It shows that the linear-to-nonlinear lift transition angle at Re=1×10^4 is reduced from α=9° to around α=5° compared with Re=3×10^3.

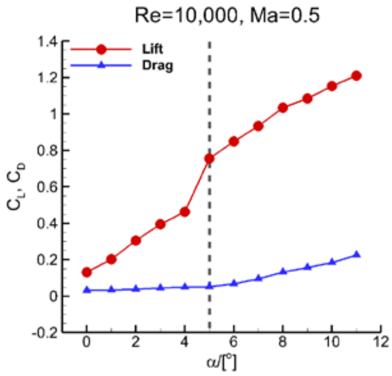

Figure 14: Time-averaged lift and drag coefficients at Re=1×10^4 (α=0°~11°)

Instantaneous three-dimensional vortical structures around α=5° are visualized with an iso-surface of the Q-criterion in Figure 15. It can be observed that at a Reynolds number of 1×10^4, a spanwise instability becomes apparent. Large two-dimensional spanwise vortices break down into small three-dimensional streamwise vortices. As the time-averaged flow fields and contours of the turbulent kinetic energy show in Figure 16 and Figure 17, respectively, the turbulence develops gradually with an increase of angle of attack. At α=4°, the flow upstream the apex is attached but a relatively large separation zone is developed downstream the apex (as shown in Figure 16) and the separated shear-layer breaks into 3D vortex structures in the wake region. At α=5°, two small separation zones can be observed upstream and downstream the apex respectively. Compared with the case of α=4°, the breakup of the shear-layer is delayed and the fluctuation intensity is reduced (as shown in Figure 17), probably due to the reduction of size of the downstream separation zone.

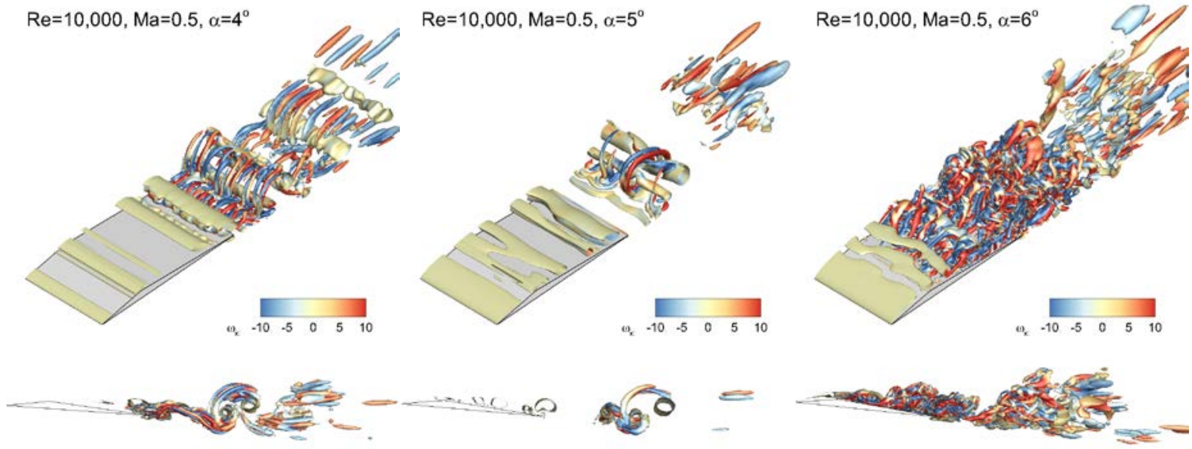

Figure 15: Instantaneous iso-surfaces of Q=10 at Re=1×10^4 (α=4°~6°)

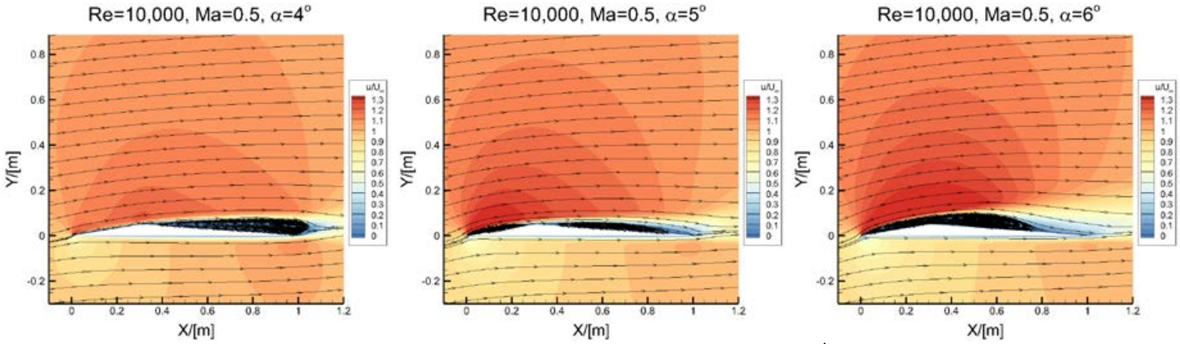

Figure 16: Time-averaged flow fields at Re=1×10^4 (α=4°~6°)

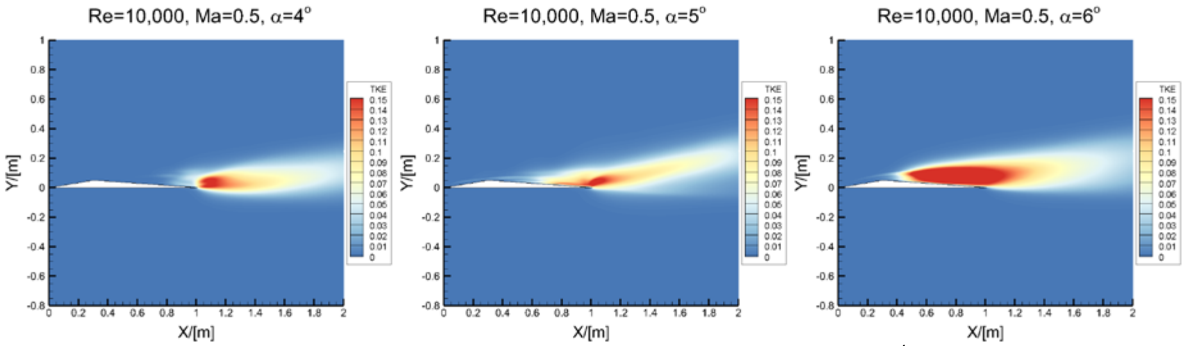

Figure 17: Contours of the turbulent kinetic energy at Re=1×10^4 (α=4°~6°)

4 Conclusions and Future Work

Direct numerical simulations of a triangular airfoil designed for operating in theMartian atmosphere have been conducted to study the aerodynamic characteristics of an airfoil at low Reynolds numbers, especially laminar-turbulent transition around the critical angle of attack. The code ASTR based on a compact sixth-order central scheme and tenth-order filter is used as the numerical solver. The O-grid was generated around the triangular airfoil, concentrating towards the upper surface of the airfoil to capture the laminar separation and subsequent turbulence. Two Reynolds numbers are studied at Re=3×10^3 and 1×10^4 with a Mach number of M=0.5, and angle of attack changing from α=0° to 18° and α=0° to 11°, respectively.

A nonlinear variation of lift coefficients with AoA is observed at both Reynolds numbers. From the time-averaged flow fields obtained by three-dimensional DNS, it shows that the linear-to-nonlinear transition is caused by the transition of three separation forms around the triangular airfoil. At Re=3×10^3, there is a recirculation zone that forms behind the apex for lower angles of attack of α≤6°. With an increase in the angle of attack (α=7°~8°), we note that a small separation bubble near the leading edge appears but without any apex separation bubble. We refer to this separation phenomenon as a double bubble separation. These two separation bubbles merge into a large leading-edge separation bubble when the angle of attack is increased to α=9°. The recirculation zone grows and covers the majority of the airfoil for higher angles of attack.

The effect of higher Reynolds numbers on flow fields around the airfoil is shifting the transition angle of attack to be lower. The results for Re=1×10^4 show that the turbulence develops gradually with the increase of AoA. At α=4°, the flow upstream the apex is attached but a relatively large separation zone is developed downstream of the apex and the separated shear-layer breaks into 3D vortex structures in the wake region. At α=5°, two small separation zones can be observed upstream and downstream the apex, respectively. Compared with the case of α=4°, the breakup of the shear-layer is delayed and the fluctuation intensity is reduced, probably due to the reduction of size of the downstream separation zone. With a further increase of AoA, a fully separated flow is observed and turbulence is developed above the airfoil. Further analysis of the flow physics around the airfoil under different conditions, such as Mach number and specific heat ratio, are on-going.

Acknowledgments

The authors gratefully acknowledge the computing time granted by the Engineering and Physical Sciences Research Council (EPSRC) through the U.K. Turbulence Consortium (Grant No. EP/L000261/1) and the simulations were run on the U.K. High-Performance Computing Service ARCHER. DRE gratefully acknowledges additional support from EPSRC under grants “Nano-Engineered Flow Technologies: Simulation for Design across Scale and Phase” (EP/N016602/1), and grants EP/L00030X/1 and EP/K038451/1.

References

[1] M. Galbraith, M. Visbal. Implicit Large Eddy Simulation of Low-Reynolds-Number Transitional Flow past the SD7003 Airfoil. AIAA 2010-4737, 2010.
[2] M. Okamoto, A. Azuma. Experimental Study on Aerodynamic Characteristics of Unsteady Wings at Low Reynolds Number. AIAA Journal, 43(12):2526-2536, 2005.
[3] P. Munday, K. Taira, T. Suwa, et al. Nonlinear Lift on a Triangular Airfoil in Low-Reynolds-Number Compressible Flow. Journal of Aircraft, 52(3):924-931, 2015.
[4] A. Uranga, P.-O. Persson, M. Drela, et al. Implicit Large Eddy Simulation of Transitional Flows over Airfoils and Wings. 19th AIAA Computational Fluid Dynamics, 2009, AIAA 2009-4131.
[5] P. D. Boom and D. W. Zingg. Time-Accurate Flow Simulations Using an Efficient Newton-Krylov-Schur Approach with High-Order Temporal and Spatial Discretization. 51st AIAA Aerospace Sciences Meeting including the New Horizons Forum and Aerospace Exposition, 2013, AIAA 2013-0383.
[6] C. Carton de Wiart and K. Hillewaert. DNS and ILES of transitional flows around a SD7003 using a high order Discontinuous Galerkin method. Seventh International Conference on Computational Fluid Dynamics, 2012, ICCFD7-3604.
[7] M. Galbraith. Implicit Large Eddy Simulation of Low-Reynolds-Number Transitional Flow past the SD7003 Airfoil. Master's thesis, University of Cincinnati, 2009, AIAA 2010-4442.
[8] D. Garmann, M. Visbal, and P. Orkwis. Comparative study of implicit and subgrid-scale model large-eddy simulation techniques for low-Reynolds number airfoil applications. Int. J. Number. Meth. Fluids, 2012, 71:1546-1565.
[9] Y. Zhou, and Z. Wang. Implicit Large Eddy Simulation of Transitional Flow over a SD7003 Wing Using High-Order Spectral Difference Method. 40th Fluid Dynamics Conference and Exhibit, 2010, AIAA 2010-4442.
[10] P. Castonguay, C. Liang, and A. Jameson. Simulation of Transitional Flow over Airfoils using the Spectral Difference Method. 40th Fluid Dynamics Conference and Exhibit, 2010, AIAA 2010-4626.
[11] V. Skarolek, and K. Miyaji. Transitional Flow over a SD7003 Wing Using Flux Reconstruction Scheme. 52nd Aerospace Sciences Meeting, 2014, AIAA 2014-0250.
[12] R. Radespiel, J. Windte, and U. Scholz. Numerical and Experimental Flow Analysis of Moving Airfoils with Laminar Separation Bubbles. 2006, AIAA 2006-501.
[13] M. Ol, B. McAuliffe, E. Hanff, et al. Comparison of Laminar Separation Bubble Measurements on a Low Reynolds Number Airfoil in Three Facilities. AIAA Paper, 2005-5149, June, 2005.
[14] A. Uranga. Investigation of transition to turbulence at low Reynolds numbers using Implicit Large Eddy Simulations with a Discontinuous Galerkin method. Ph.D. thesis, Massachusetts Institute of Technology, 2011.
[15] D. Garmann, and M. Visbal. High-order solutions of transitional flow over the SD7003 airfoil using compact finite-differencing and filtering. AIAA 1st International Workshop on High-Order CFD Methods, 2012.
[16] B. Zimmerman, and Z. Wang. Transitional Flow Over an SD7003 Wing. AIAA 1st International Workshop on High-Order CFD Methods, 2012.

[17] R. Hain, C. Kahler, and R. Radespiel. Dynamics of laminar separation bubbles at low-Reynolds-number aerofoils. Journal of Fluid Mechanics, 630:129-153, 2009.
[18] Y. Lian, and W. Shyy. Laminar-turbulent transition of a low Reynolds number rigid or flexible airfoil. AIAA Journal, 45(7):1501-1513, 2007.
[19] W. Yuan, M. Khalid, J. Windte, et al. An investigation of low-Reynolds-number flows past airfoils. 23rd AIAA Applied Aerodynamics Conference, 2005, AIAA 2005-4607.
[20] S. Deng, L. Jiang, C. Liu. DNS for flow separation control around an airfoil by pulsed jets. Computers & Fluids 36 (2007) 1040–1060.